Significant N-containing brown carbon emission from heavy-duty diesel vehicles revealed by the molecular and chromophore analysis using ultra-high resolution mass spectrometry

Xiao He[1], Xuan Zheng[1*], Bin Jiang[2], Xubing Cao[3], Ting Chen[1], Shuwen Guo[1], Zhiyuan Li[4], Yan Ding[5,6], Shaojun Zhang[7,8*], Yuan Cheng[3], Jingkun Jiang[7,8], Shuxiao Wang[7,8], and Ye Wu[7,8]

[1]College of Chemistry and Environmental Engineering, Shenzhen University, Shenzhen 518060, China

[2]State Key Laboratory of Organic Geochemistry, Guangzhou Institute of Geochemistry, CAS, Guangzhou 510640, China

[3]State Key Laboratory of Urban Water Resource and Environment, School of Environment, Harbin Institute of Technology, Harbin, 150090, China

[4]School of Public Health (Shenzhen), Sun Yat-sen University, Guangzhou 510275, China

[5]State Environmental Protection Key Laboratory of Vehicle Emission Control and Simulation, Chinese Research Academy of Environmental Sciences, Beijing 100012, China

[6]Vehicle Emission Control Center, Chinese Research Academy of Environmental Sciences, Beijing 100012, China

[7]School of Environment, State Key Joint Laboratory of Environment Simulation and Pollution Control, Tsinghua University, Beijing 100084, China

[8]State Environmental Protection Key Laboratory of Sources and Control of Air Pollution Complex, Beijing 100084, China

The supporting information includes 4 texts: information about the recruited HDDVs, dynamic sampling of field blanks and the quality control/quality assurance, calculation of the double bond equivalent (DBE), oxidation state of carbon atoms [1], the aromaticity index (AI), the modified AI_{mod}, and Kendrick Mass Defect (KMD) based on CH2, and calibration of FT-ICR MS

Number of pages: 8

Number of figures: 7

Number of tables: 3

S1. Information about the recruited HDDVs

Two in-use heavy-duty diesel vehicles (HDDVs) were recruited for chassis dynamometer testing and modeled in the year of 2020 (vehicles D1 and D2). Both vehicles, equipped with selective catalytic reduction (SCR) systems, meet the China V emission standard and have a gross vehicle weight of 25 tons. Vehicle models, weights, and after-treatment technologies are summarized in Table S1.

S2. Dynamic sampling of field blanks and the quality control/quality assurance

Field blanks of background dilution air were collected in parallel with sample collection to account for background contamination. Filtered ambient air was drawn into the constant volume sampler (CVS, MEXA-7200DTR) and deposited on quartz filter over a 30-min period. These blanks were included in all analyses to ensure data integrity and correct for any potential background contamination.

S3. Calculation of the double bond equivalent (DBE), oxidation state of carbon atoms [1], the aromaticity index (AI), the modified AI_{mod}, and Kendrick Mass Defect (KMD) based on CH2

We used FT-ICR MS to derive these molecular metrics. For a molecular formula $C_cH_hO_oN_nS_s$, its DBE, OSc,[2] AI, AI_{mod}[3] , X_c[4], and KMD values based on CH2 are calculated as follows:

$$DBE = \frac{2 \times c + 2 - h + n}{2}$$

$$OSc \approx 2 \times \frac{o}{c} - \frac{h}{c} - 5 \times \frac{n}{c} - 6 \times \frac{s}{c}$$

$$AI = \frac{1 + c - o - s - 0.5 \times h}{c - o - s - n}$$

$$AI_{mod} = \frac{1 + c - 0.5 \times o - s - 0.5 \times h}{c - 0.5 \times o - s - n}$$

$$X_c = \frac{2C + N - H - 2mO}{DBE - mO} + 1$$

$$\mathrm{KMD_{based\ on\ CH_2}} = \mathrm{Roundup}\left(\mathrm{Mass} \times \frac{14}{14.01565}\right) - \mathrm{Mass} \times \frac{14}{14.01565}$$

These metrics provide crucial insights into the degree of unsaturation, aromaticity, and oxidation state, to understand the reactivity and environmental implications of BrC.

S4. Calibration of FT-ICR MS

FT-ICR MS was calibrated externally using a homologous series of N_1 and O_2 compounds, e.g., $C_{16}H_{21}O_2$, $C_{17}H_{33}O_2$, $C_{18}H_{35}O_2$, to ensure the mass accuracy of the measurement results. It was recalibrated internally with typical class species peaks using quadratic calibration in DataAnalysis 5.0 (Bruker Daltonics GmbH & Co. KG, Bremen, Germany). The high mass accuracy achieved in FT-ICR MS facilitated precise molecular formula assignments, enabling robust structural elucidation of BrC components.

S5. Measurement of light absorption and the mass absorption efficiency (MAE)

A precise portion of the filter was cut and extracted in 50/70 mL methanol (Chromatographic grade) under sonication for 1 h. The extracts were subsequently filtered through a PTFE membrane (0.45 μm, Pall Corporation, NY) to remove any insoluble substances. Light absorption spectra, ranging over 200-800 nm, were measured using a 2.5 m long-path liquid waveguide capillary cell (LWCC-3250, World Precision

Instruments, USA) coupled with a UV-Visible spectrophotometer (Ocean Optics). Light absorption of pure methanol was treated as the baseline absorption. LWCC was washed thoroughly with methanol after each sample analysis to prevent carry-over effects.

The light absorption coefficient (b_{abs}, Mm^{-1}) is described by the following equation:[5]

$$b_{abs} = (A_\lambda - A_{700}) \times \frac{V_{solution}}{V_{air} \times L} \times \ln 10 \times 10^6 \quad (1)$$

where A_λ is the absorbance at a given wavelength; A_{700} is the absorbance at 700 nm to account for any baseline drift; $V_{solution}$ (L) is the volume of the solution in which the filter was extracted; V_{air} (L) is the air volume sampled through the filter. The absorbing path length L is 2.5 m.

The absorption Ångström exponent (AAE) is a measure of the absorption wavelength dependence and was determined by constructing a linear regression fit to the logarithms of $b_{abs,\lambda}$ and wavelength. The wavelength range of 300-450 nm was used for the linear regression fit. The $b_{abs,\ 365\ nm}$, AAE (300−450 nm), and the regression coefficient (R^2) for the selected samples are shown in Table S3. The AAE values range from 5.97 to 6.97, aligning with previously reported AAE for vehicle emissions.[6, 7] The mass absorption efficiency (MAE, m^2/gC) of BrC, which represents the absorption capacity, is calculated as follows:

$$MAE = \frac{b_{abs}}{Conc.\ of\ OC} \quad (2)$$

The concentration of methanol-extracted OA was derived from the organic carbon (OC) concentration measured by the carbon analyzer, with a conversion factor of 0.85 applied.[8]

S6. Measurement of OC, elemental carbon (EC), and total carbon (TC)

A filter of 0.552 cm^2 was precisely cut, placed in the sample oven, and analyzed by a thermal-optical analysis (TOA) method using a carbon analyzer (Model 2001, Desert Research Institute, USA) following the IMPROVE-A protocol. The laser source was a Helium-Neon laser at 633 nm, and the carbon detector was the flame ionization detector (FID). The working principle of the analyzer is based on the preferential oxidation of OC and EC at different temperatures. The filter was initially heated in an inert atmosphere (100% He) where the OC constituents were vaporized at 140 °C (OC1), 280 °C (OC2), 480 °C (OC3), and 580 °C (OC4), respectively. The vaporized carbon constituents were converted to CH_4 and detected by the FID. The corrected concentration of OC is computed using the following equation:

$$Corrected\ OC = OC1 + OC2 + OC3 + OC4 + OC_{pyro} \quad (3)$$

where OC_{pyro} refers to the pyrolyzed OC formed from charring.[9] The oven was then switched to an oxidizing atmosphere (He with 10% O_2) where EC fractions were oxidized at 580 °C (EC1), 740 °C (EC2), and 840 °C (EC3). TC and EC are determined by the following equations:

$$TC = OC1 + OC2 + OC3 + OC4 + EC1 + EC2 + EC3 \quad (4)$$

$$EC = TC - OC \quad (5)$$

S7. Mass concentrations of OC and EC emitted by HDDVs under different driving conditions

The emissions of OC and EC from the tested HDDVs under different driving conditions are shown in Figure S2. The average OC concentrations during the cold-start and hot-start driving conditions at room temperature (approximately 25 °C) were 27.4 ± 10.0 μg/m^3 and 23.9 ± 5.7 μg/m^3 for D1, and 35.6 ± 0.3 μg/m^3 and 19.8 ± 1.0 μg/m^3 for D2, respectively. OC emissions decreased by 12% and 44% under hot-start driving conditions

compared to cold-start conditions for D1 and D2. The average OC concentrations at 0 °C were 25.6 μg/m^3 and 20.4 μg/m^3 under cold-start and hot-start driving conditions, indicating an emission reduction of 28% under cold-start driving and an increase of 3% under hot-start driving compared to tests conducted at 25 °C. Similar trends were observed for EC emissions, with reductions of 16% and 73% under hot-start conditions compared to cold-start conditions for D1 and D2. Consistent with OC, EC emissions at low temperatures showed a 38% reduction, whereas a substantial increase of 101% in EC emissions at 0 °C was observed during the hot-start phase. Song et al. (2023) reported the enhanced emissions of both OC and EC for HDDVs when ambient temperatures dropped to -20 °C.[10] The discrepancy could be attributed to the extremely low temperature in the referenced work, the small sample sizes, and the differences in emission standards. China II and China IV HDDVs were deployed in their tests and the emission enhancement at -20 °C was significantly reduced from China II to China IV vehicles. It is worth noting that the effects of ambient temperature on vehicle emissions are complex and it is hasty to quantify them using chassis dynamometers or portable emission measurements systems, as these approaches rely on testing a relatively small number of vehicles.

Table S1. Synopsis information of the tested vehicles.

Vehicle ID	Vehicle type	Emission standard	Aftertreatment devices	Model year	Curb weight (t)	Gross vehicle weight (t)
D1	Semi-trailer tractor	China V	SCR*	2021.05	8.8	25
D2	Semi-trailer tractor	China V	SCR	2021.04	8.8	25

*SCR: Selective catalytic reduction

Table S2. List of experiments for each vehicle and driving condition.

	Vehicle	Test environment	Start	FT-ICR	OC/EC	Light absorption spectra
20211222-1	D1	25 °C	Cold	POS + NEG	Y	Y
20211222-2	D1	25 °C	Hot	POS + NEG	Y	Y
20211223-1	D1	25 °C	Cold	POS + NEG	Y	Y
20211223-2	D1	25 °C	Hot	POS + NEG	Y	Y
20211224-1	D1	25 °C	Cold	POS + NEG	Y	Y
20211224-2	D1	25 °C	Hot	POS + NEG	Y	Y
20211227-1	D2	25 °C	Cold	POS + NEG	Y	Y
20211227-2	D2	25 °C	Hot	POS + NEG	Y	Y
20211228-1	D2	25 °C	Cold	POS + NEG	Y	Y
20211228-2	D2	25 °C	Hot	POS + NEG	Y	Y
20211228-3^	D2	25 °C	Hot	POS + NEG	Y	Y
20211229-1	D2	25 °C	Cold	POS + NEG	Y	Y
20211229-2	D2	25 °C	Hot	POS + NEG	Y	Y
20211229-3	D2	0 °C	Cold	POS + NEG	Y	Y
20211229-4	D2	0 °C	Hot	POS + NEG	Y	Y
20211229-5	D2	0 °C	Hot	POS + NEG	Y	Y
Blk1#		25 °C		POS + NEG	Y	Y
Blk2		25 °C		POS + NEG	Y	Y
Blk3		25 °C		No*	Y	Y

*No result due to technical issue

#Field blank sample

^10-min sample

Table S3. The $b_{abs,\ 365\ nm}$, absorption Ångström exponent (AAE, 300-450 nm) and the regression coefficient (R^2) of the selected samples.

Sample ID	20211222-1				20211228-1
Driving condition	P1	P2	P3	Full	Full
$b_{abs,\ 365\ nm}$ (Mm^{-1})	5.13	4.08	4.12	3.18	1.81
AAE (300-450 nm)	6.01	6.56	5.97	6.97	6.65
R^2	0.99	0.98	0.98	0.99	0.97

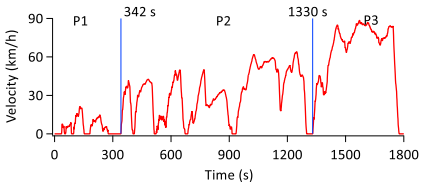

123

124 Figure S1. Speed trace for CHTC-HT cycle. The whole duration is 1800 s and divided into three phases:
125 low-speed (P1), middle-speed (P2), and high-speed (P3). The time intervals are 342 s, 988 s, and 470 s,
126 respectively.

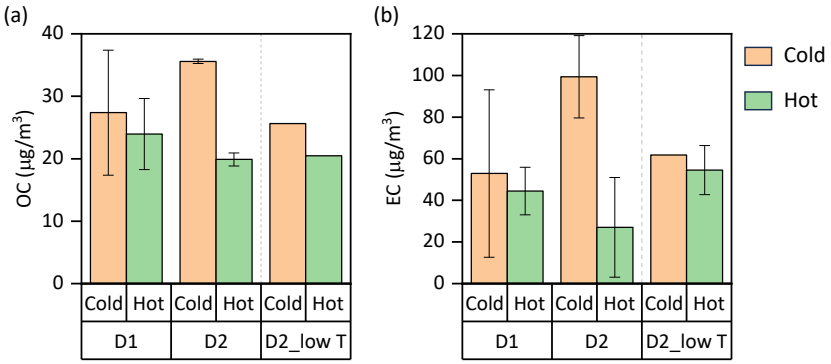

127

128 Figure S2. Emissions factors of OC and EC from the tested HDDVs under different driving conditions.

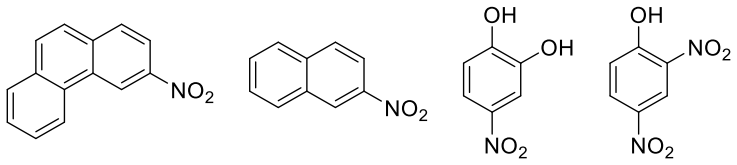

129

130 Figure S3. Representative chemical structures with conjugated oxygenated groups when discussing the
131 optical properties of BrC.

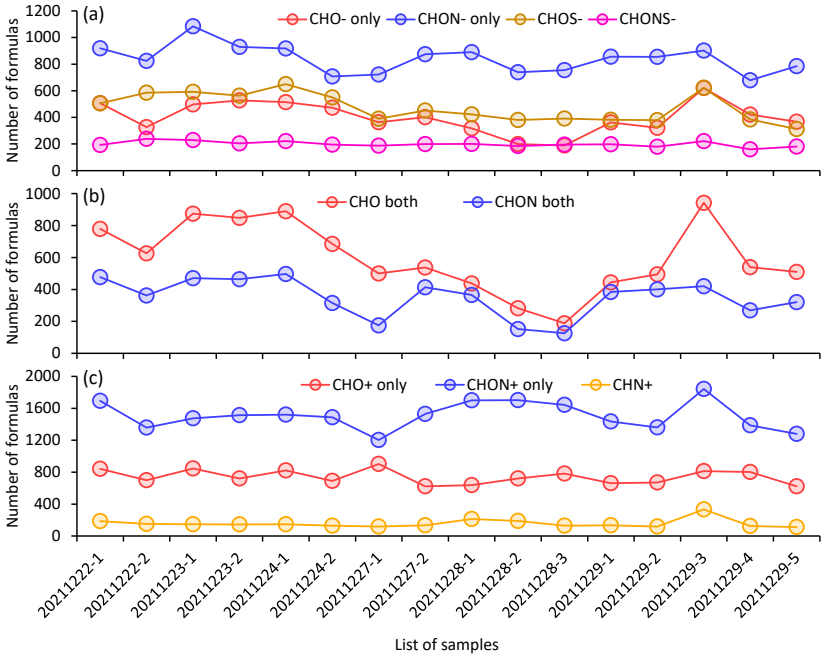

Figure S4. The number of formulas detected in (a) negative mode, (b) both modes, and (c) positive mode in individual samples.

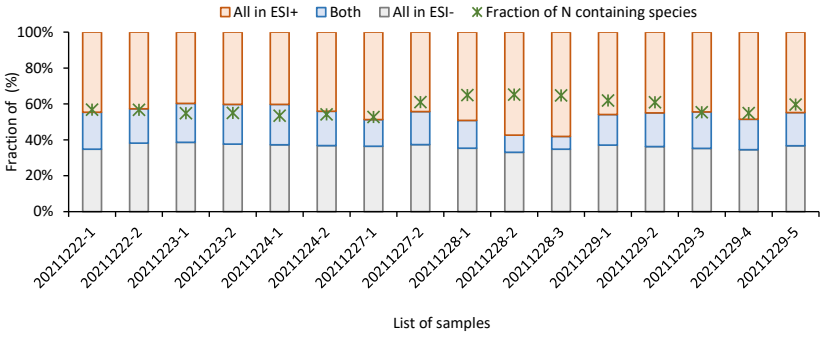

Figure S5. The fraction of formulas detected in negative mode, both modes, and positive mode in individual samples and the respective fraction of N-containing species.

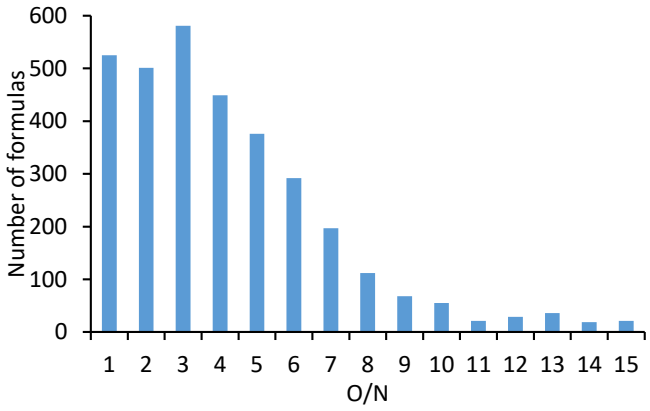

Figure S6. The number of CHON formulas identified in the representative sample of 20211211-1, divided into subgroups of different O/N ratio.

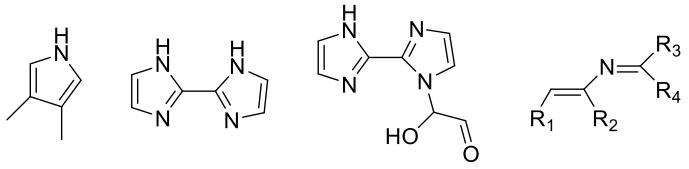

Figure S7. Example chemical structures with C=N and C-N functional groups as the bonding structures of BrC.

References:

(1) Schwanz, T. G., Nespeca, M. G., Cardoso Dias, J., Valadão Vieira Bokowski, L., Marcelo, M. C. A., Maximiano, D. H., Santos Canova, L., Brasil de Souza Cruz, P., Swenson Pontes, O. F., Kaiser, S. GC × GC-TOFMS and chemometrics approach for comparative study of volatile compound release by tobacco heating system as a function of temperature. *Microchemical Journal* **2020**, *159*, 105578. https://www.sciencedirect.com/science/article/pii/S0026265X20318750.

(2) Kroll, J. H., Donahue, N. M., Jimenez, J. L., Kessler, S. H., Canagaratna, M. R., Wilson, K. R., Altieri, K. E., Mazzoleni, L. R., Wozniak, A. S., Bluhm, H., Mysak, E. R., Smith, J. D., Kolb, C. E., Worsnop, D. R. Carbon oxidation state as a metric for describing the chemistry of atmospheric organic aerosol. *Nature Chemistry* **2011**, *3* (2), 133-139. https://dx.doi.org/10.1038/nchem.948.

(3) Koch, B. P., Dittmar, T. From mass to structure: an aromaticity index for high‐resolution mass data of natural organic matter. *Rapid Communications in Mass Spectrometry* **2006**, *20* (5), 926-932. https://dx.doi.org/10.1002/rcm.2386.

(4) Yassine, M. M., Harir, M., Dabek‐Zlotorzynska, E., Schmitt‐Kopplin, P. Structural characterization of organic aerosol using Fourier transform ion cyclotron resonance mass spectrometry: Aromaticity equivalent approach. *Rapid Communications in Mass Spectrometry* **2014**, *28* (22), 2445-2454. https://dx.doi.org/10.1002/rcm.7038.

(5) Hecobian, A., Zhang, X., Zheng, M., Frank, N., Edgerton, E. S., Weber, R. J. Water-Soluble Organic Aerosol material and the light-absorption characteristics of aqueous extracts measured over the Southeastern United States. *Atmos. Chem. Phys.* **2010**, *10* (13), 5965-5977. https://dx.doi.org/10.5194/acp-10-5965-2010.

(6) Huang, R.-J., Yuan, W., Yang, L., Yang, H., Cao, W., Guo, J., Zhang, N., Zhu, C., Wu, Y., Zhang, R. Concentration, optical characteristics, and emission factors of brown carbon emitted by on-road vehicles. *Sci. Total Environ.* **2022**, *810*, 151307. https://www.sciencedirect.com/science/article/pii/S0048969721063853.

(7) Pani, S. K., Lin, N.-H., Griffith, S. M., Chantara, S., Lee, C.-T., Thepnuan, D., Tsai, Y. I. Brown carbon light absorption over an urban environment in northern peninsular Southeast Asia. *Environ. Pollut.* **2021**, *276*, 116735. https://www.sciencedirect.com/science/article/pii/S0269749121003158.

(8) Cheng, Y., He, K.-b., Du, Z.-y., Engling, G., Liu, J.-m., Ma, Y.-l., Zheng, M., Weber, R. J. The characteristics of brown carbon aerosol during winter in Beijing. *Atmospheric Environment* **2016**, *127*, 355-364. https://www.sciencedirect.com/science/article/pii/S1352231015306075.

(9) Zhang, X., Trzepla, K., White, W., Raffuse, S., Hyslop, N. P. Intercomparison of thermal–optical carbon measurements by Sunset and Desert Research Institute (DRI) analyzers using the IMPROVE_A protocol. *Atmos. Meas. Tech.* **2021**, *14* (5), 3217-3231. https://dx.doi.org/10.5194/amt-14-3217-2021.

(10) Song, W. W., Fang, W. X., Liu, H., Li, W. L., Zhang, Z., Li, C. H., Yu, D., Zhao, Q., Wang, X. S., He, K. B. Enhanced diesel emissions at low ambient temperature: hazardous materials in fine particles. *Journal of Hazardous Materials* **2023**, *449*, 131011. https://www.sciencedirect.com/science/article/pii/S0304389423002935.